

1 **Adsorption and photocatalytic degradation of Methylene Blue over Hydrogen-Titanate**
2 **nanofibres produced by a peroxide method**

3

4 Ibrahim El Saliby¹, Laszlo Erdei², Jong-Ho Kim³ and Ho Kyong Shon^{1*}

5

6 ¹Faculty of Engineering and Information Technology, University of Technology, Sydney
7 (UTS), PO Box 123, Broadway, 2007 Australia

8 ²Faculty of Engineering and Surveying, University of Southern Queensland, QLD 4350,
9 Toowoomba, Australia

10 ³School of Applied Chemical Engineering, Chonnam National University, Gwangju 500-757,
11 Korea

12

13 Email addresses: ibrahim.elsaliby@uts.edu.au (I. El Saliby), laszlo.erdei@usq.edu.au (L.
14 Erdei), jonghkim@chonnam.ac.kr (J.-H. Kim), hokyong.shon-1@uts.edu.au (H.K. Shon),

15

16 * Corresponding author: Tel: +61 2 9514 2629, fax: +61 2 9514 2633

17

18 **Abstract**

19

20 In this study, Degussa P25 TiO₂ was partially dissolved in a mixture of hydrogen peroxide
21 and sodium hydroxide at high pH. The fabrication of nanofibres proceeded by the
22 hydrothermal treatment of the solution at 80 °C. This was followed by acid wash in HCl at
23 pH 2 for 60 min, which resulted in the formation of hydrogen-titanate nanofibres. The
24 nanofibres were annealed at 550 °C for 6 h to produce crystalline anatase nanofibres. The
25 nanofibres were characterised for physico-chemical modifications and tested for the
26 adsorption and photocatalytic degradation of methylene blue as a model water pollutant. An
27 average specific surface area of 31.54 m²/g, average pore volume of 0.10 cm³/g and average
28 pore size of 50 Å were recorded. The nanofibres were effective adsorbents of the model
29 pollutant and adsorbents and good photocatalysts under simulated solar light illumination. No
30 reduction in photocatalytic activity was observed over three complete treatment cycles, and
31 the effective separation of nanofibres was achieved by gravity settling resulting in low
32 residual solution turbidity.

33

34 **Keywords:** water purification, adsorption, nanofibres, photocatalysis, titanium dioxide,
35 hydrogen peroxide.

36

37 **1. Introduction**

38

39 The use of titania nanoassemblies in the treatment of contaminated water have provided a
40 solution to the problem encountered during the separation of nanoparticles from water. Even
41 though “traditional” nanoparticles showed better apparent photocatalytic activity, their
42 separation from the suspension remains the major challenge for process up-scaling.
43 Therefore, the use of relatively large titanate nanoassemblies has become more popular
44 because they can be easily removed from the solution.

45

46 The production of titanate nanostructures using a peroxo-titanate solution has been discussed
47 by several authors (Mao et al., 2006; Nyman and Hobbs, 2006), and the application of Na-
48 titanates in the adsorption and photocatalytic removal of Methylene Blue (MB) was recently
49 reported (El Saliby et al., 2011a). Titanate nanostructures can effectively adsorb dye
50 molecules due to their high surface area and special characteristics (Lee et al., 2007; Baiju et
51 al., 2009; Xiong et al., 2010). The effect of synthesis temperature (Lee et al., 2008a), and
52 sodium content (Lee et al., 2008b) on the cation exchange capacity of titanate nanotubes were
53 reported. It was found that the increase of sodium content in the nanotubes increases the
54 adsorption of dye through cationic exchange. Na^+ can be replaced by H^+ in the nanostructure
55 framework by washing the Na-titanates in an HCl solution (Wei et al., 2004; Zhu et al., 2004;
56 Mao et al., 2006; Bela et al., 2010). Bela et al. (2010) reported that the ion exchange in the
57 titanate nanobelts was highly dependent on the duration of acid wash. The authors found that
58 the acid wash of titanate nanobelts in a 0.1 M HCl solution for 72 h was enough to
59 completely exchange Na^+ for H^+ .

60

61 The adsorption of MB on TiO_2 nanoparticles from aqueous solution was studied by Fetterolf
62 et al. (2003). The authors found that the Langmuir adsorption model is adequate for
63 representing the adsorption of MB, which was attributed to electrostatic attractions. Similarly,
64 Xiong et al. (2010) studied the adsorption of MB on titanate nanotubes and reported that the
65 Langmuir model was appropriate for describing the monolayer adsorption mechanism.

66

67 In a recent study, MB adsorption on titanate nanostructures has been found to significantly
68 affect the degradation of the dye under UV light (Xiong et al., 2011). Better photocatalytic
69 decomposition was achieved in the adsorption/photocatalysis system compared to the
70 adsorption followed by photocatalysis system under UV irradiation. The adsorption of dye
71 molecules onto titanate nanostructures can be of significant importance in terms of initiating
72 the dye sensitization mechanism. This can be used in solar light treatment systems that treat
73 dye contaminated wastewater. Thus, the objectives of this study were to:

- 74 ➤ Synthesise H-titanates nanofibres by a peroxide method and study their morphology
75 and physico-chemical characteristics.
- 76 ➤ Investigate the kinetics of MB adsorption on the nanofibres and carry out
77 photocatalytic degradation of MB under simulated solar light.
- 78 ➤ Test the photocatalytic stability and the ease of separation of the produced
79 nanofibres.

80

81 **2. Experimental Investigations**

82 **2.1. Synthesis**

83

84 H-titanate nanofibres were fabricated by the same method described elsewhere (El Saliby et
85 al., 2011b). In a typical synthesis, 2 g of Degussa P25 powder was dispersed in 12 mL of
86 H₂O₂ (50%) under alkaline conditions by adding 4 g of NaOH (final pH 13). Later on, the
87 mixture was placed in a Teflon cell at 80 °C for 24 h. After hydrothermal treatment, the pH
88 of the Na-titanates suspension was decreased to pH 2 by using 1 N HCl, at which ion
89 exchange (Na⁺ and H⁺) was carried out for 60 min under magnetic stirring. This was followed
90 by washing with Milli Q (MQ) water until a pH of 7. The as-prepared nanofibres were dried
91 in oven at 100 °C for 12 h and annealed at 550 °C for 6 h to obtain anatase nanofibres. H-
92 titanate anatase nanofibres will be named hereafter as HTNF.

93

94 **2.2. HTNF Characterisation**

95

96 Morphology and elemental composition analyses of HTNF were carried out using the Zeiss
97 Supra 55VP SEM/EDS operating at 20 kV. X-ray diffraction (XRD) patterns were generated
98 on MDI Jade 5.0 X-ray diffractometer. Brunauer, Emmet and Teller (BET) surface area
99 analyses were performed on an automated surface area analyser (Micromeritics Gemini 2360,
100 USA) by means of nitrogen adsorption-desorption. The zeta potential of as-prepared and

101 calcined powders was determined by dispersing the nanofibres in MQ water under variable
102 pH (adjusted by 0.1 N HCl or NaOH) and measured using the Malvern nano-series (Nano-zs,
103 Malvern Instruments Limited, UK) analyser.

104

105 **2.3. MB Adsorption Experiments**

106

107 MB powder was dissolved in MQ water to prepare a stock solution of 1 g/L concentration.
108 All experimental MB solutions were prepared from the stock solution by dilution. The dark
109 adsorption experiments were performed in 250 mL conical glass Erlenmeyer flasks
110 containing 100 mL of the desired MB solution. The flasks were enwrapped in aluminium foil
111 to prevent the illumination of slurries by ambient light. The homogeneity of suspensions was
112 maintained by placing the flasks in an orbital shaking incubator (Thermoline, TU400) at a set
113 temperature of 25 °C and a shaking speed of 150 rpm unless otherwise stated. Samples were
114 collected at designated time intervals, filtered through 0.45 µm polytetrafluoroethylene
115 (PTFE) membrane syringe filters, and analysed for colour removal by measuring absorbance
116 at the maximum absorbance wavelength of MB ($\lambda = 664$ nm) using a Shimadzu UV-Vis 1700
117 spectrophotometer. The concentration of MB (mg/L) was calculated by the following
118 equation:

119

$$120 \quad C_t = \frac{Abs_t}{Abs_0} C_0 \quad (Eq. 1)$$

121

122 where, C_t (mg/L) is the concentration of MB at time t , C_0 (mg/L) is the initial concentration
123 of MB, Abs_t and Abs_0 are absorbance values for $\lambda = 664$ nm at time t and 0, respectively.

124

125 **2.3.1. Effect of HTNF Loading**

126

127 In this experiment, five different powder loadings (0.1, 0.2, 0.5, 1 and 2 g/L) were selected to
128 study the adsorption of MB molecules onto HTNF. The experimental conditions were: MB
129 concentration 10 mg/L, pH = 9 (after adding the powder no pH adjustment was done) and T =
130 25 °C.

131

132 **2.3.2. Effect of MB Concentration**

133

134 After optimising the HTNF loading, three MB concentrations (5, 10 and 20 mg/L) were
135 selected to study the kinetics of adsorption. The experiment was performed under the
136 following conditions: HTNF = 0.5 g/L, pH = 9 and T = 25 °C.

137

138 2.3.3. Effect of pH

139

140 The pH of the solution is known to affect the surface charge of the nanofibres, and
141 consequently the adsorption of dye molecules. The experiment was conducted at the pH
142 values of 3, 5, 7 and 9 while all other factors were kept constant at HTNF = 0.5 g/L, MB = 20
143 mg/L and T = 25 °C.

144

145 2.3.4. Effect of Solution Temperature

146

147 The temperature of the solution was changed to study its effect on the adsorption process. In
148 these experiments the selected temperatures were 25, 35, and 45 °C. The experimental
149 conditions were: HTNF = 0.5 g/L, MB = 20 mg/L, and pH = 9.

150

151 2.3.5. Adsorption Equilibrium and Isotherms

152

153 The amount of dye adsorbed at equilibrium was calculated from the following equation:

154

$$155 \quad q_e = (C_0 - C_e) \frac{V}{m} \quad (\text{Eq. 2})$$

156

157 where, C_0 and C_e (mg/L) are the initial and equilibrium concentration of MB in solution, V
158 (L) is the solution volume and m (g) is the mass of the HTNF.

159

160 Sorption equilibrium data were fitted to the Langmuir, Freundlich, and Toth models using
161 both linearised and nonlinear parameter estimations. The Langmuir isotherms showed good
162 correlations, while the Toth model showed significantly low fit ($R^2 = 0.70$) for HTNF loading
163 data. The Freundlich model poorly predicted the effect of MB concentration ($R^2 = 0.48$), and
164 was inappropriate ($R^2 = 0.09$) for HTNF loading data. Therefore, in this study the Langmuir
165 isotherm model was employed for data analysis, using a simple yet sufficiently accurate
166 linearised form (Langmuir, 1918):

167
168

$$\frac{C_e}{q_e} = \frac{1}{kq_m} + \frac{1}{q_m} C_e \quad (\text{Eq. 3})$$

170

171 where, C_e is the equilibrium concentration, q_e (mg/g) is the amount of adsorbate adsorbed on
172 unit mass of adsorbent, q_m (mg/g) and k (L/mg) are the Langmuir adsorption constants related
173 to adsorption capacity and rate of adsorption, respectively. The q_m and k values were
174 calculated from the slope and intercept of the straight line obtained after plotting C_e/q_e against
175 C_e , respectively.

176

177 **2.4. Photocatalytic Degradation under Simulated Solar Light**

178

179 The photocatalytic activity of HTNF (0.5 g/L) was assessed using 200 mL volume of MB
180 solution (20 mg/L). The HTNF loading and MB concentration were selected based on the
181 results obtained in the adsorption experiments. The effect of solution pH (3, 5, 7 and 9) and
182 solar light intensity (5000, 15000 and 28000 lx; measured by a digital power meter AR 823)
183 on the removal of MB were studied. MB molecules were adsorbed on HTNF in dark after
184 mixing at 450 rpm for 30 min. The solution was then placed in the Solar Simulator (SolSim,
185 Luzchem Research, Canada) and photocatalysis was carried out for 180 min at a stable
186 temperature of 26 °C. The Luzchem Research SolSim Xenon photoreactor featured an
187 enclosed exposure chamber, an exhaust system and thermostatic control to maintain the
188 chamber temperature close to ambient temperature. The principal light source was a Xenon
189 lamp (300 W) and a complex filter system ensured emission to closely match the AM1.5
190 spectrum. Air sparging was adjusted at 0.6 L/min to provide adequate dissolved oxygen to the
191 reaction. MB degradation was monitored by collecting samples (filtered by 0.45 µm PTFE
192 syringe filters) at fixed time intervals and analysed for colour removal at $\lambda = 664$ nm using a
193 Shimadzu UV-Vis 1700 spectrophotometer. Samples were also analysed for dissolved
194 organic carbon (DOC) removal using a Multi N/C 3100, Analytik Jena instrument. The
195 kinetics of the photocatalytic discolouration (MB removal) and mineralisation (DOC
196 removal) reactions were analysed by nonlinear data fitting (OriginPro v8 software,
197 OriginLab) to the equation:

198

$$199 \quad C_t = C_0 \cdot e^{-k_d \cdot t} \quad (\text{Eq. 4})$$

200

201 where, C_t (mg/L) is the concentration of MB or DOC at time t , C_0 (mg/L) is the initial
202 concentration of MB or DOC, t is time, and k_a is the apparent pseudo first order constant.

203

204 **2.5. Photocatalytic Stability**

205

206 The photocatalytic stability of HTNF (0.5 g/L) was examined over three successive cycles
207 using 200 mL volume of MB solution (20 mg/L). The pH of the solution was 9 and air
208 sparging was adjusted to a rate of 0.6 L/min at a light intensity of 28000 lx. At the end of
209 each cycle (for 8 h to ensure complete regeneration), HTNF were recovered and washed with
210 MQ water before being used in the next degradation cycle. Samples were also analysed for
211 changes in absorbance at 254 nm and 664 nm wavelengths, and for DOC removal.

212

213 **2.6. Photocatalyst Separation by Settling**

214

215 The separation of HTNF in MQ water by gravity settling was studied in 200 mL beaker by
216 collecting samples from 5 cm below the water surface (HTNF = 0.5 g/L, pH = 9). Sample
217 turbidity was logged over time and measured using the Hach HI 93414 turbidity and chlorine
218 meter.

219 **3. Results and Discussion**

220 **3.1.1. Characteristics of H-titanate Nanofibres**

221

222 Figure 1 shows the zeta potential of the as-prepared and calcined HTNF. The calcination
223 shifted the PZC towards higher pH due to the evaporation of peroxy groups (O_2^- , adsorbed
224 H_2O_2 etc). While the properties of the as-prepared titanate will not be discussed in this study,
225 its zeta potential characteristics are useful to elucidate the noticed shift of pH after
226 calcination.

227

228 SEM images of HTNF revealed fibrous nanostructures of randomly dispersed nanofibres with
229 an average diameter of 40-70 nm and few hundred nanometers in length (Figure 2). The
230 length and width of nanofibres were averaged from twenty measurements recorded after
231 image capture using a measuring tool provided by the Zeiss Supra 55VP SEM/EDS
232 instrument software. It has been discussed previously (El Saliby et al., 2011a) that the Na-
233 titanate nanofibres were arranged in microspheres of few micrometres in diameter. In
234 contrast, the acid wash at low pH (ion exchange) affected the aggregation of nanofibres but
235 the nanofibres conserved their typical morphology; the latter has also been observed by
236 several researchers (Wei et al., 2004; Zhu et al., 2004; Bela et al., 2010).

237

238 **Figure 1**

239

240 **Figure 2**

241

242 The characteristic peaks in the EDS spectrum of HTNF (Figure 3) reveal the presence of only
243 titanium and oxygen. This result indicates the effective exchange of Na^+ for H^+ prior to
244 calcination.. The XRD analysis showed that the nanofibres were mainly anatase (data not
245 shown). The calculated surface area of nanofibres was $31.54\text{ m}^2/\text{g}$, the average pore volume
246 $0.10\text{ cm}^3/\text{g}$ and average pore size 50 \AA .

247

248 **Figure 3**

249

250 **3.1.2. Effect of Operating Conditions on MB Adsorption**

251 **3.1.2.1. Effect of HTNF Loading**

252

253 The effect of HTNF loading on the removal of MB from the solution was studied using
254 photocatalyst loadings of 0.1, 0.2, 0.5, 1 and 2 g/L. The results of experiments carried out at
255 25 °C and 10 mg/L of MB are shown in Figure 4. The adsorption of MB increased with
256 photocatalyst loading until equilibrium was reached after 30 min. An increase in HTNF
257 dosage from 0.1 to 0.5 g/L increased the adsorption of MB from 11% to a remarkably high
258 90%. The increase in the adsorption efficiency can be explained by the increase in the surface
259 area available for adsorption. However, no significant increase in adsorption was recorded
260 after increasing the loading to 1 and 2 g/L (92% and 93%, respectively). This could be
261 attributed to the attainment of adsorption equilibrium between MB and HTNF, or reaching
262 the adsorption saturation point. The photocatalyst loading of 0.5 g/L was considered optimum
263 and was adopted for the next optimisation process.

264

265 **Figure 4**

266

267 3.1.2.2. Effect of Initial MB Concentration

268

269 Figure 5 shows the adsorption of MB onto HTNF using initial MB concentrations of 5, 10
270 and 20 mg/L. It is evident that the initial MB concentration played a significant role in the
271 adsorption process, where 97%, 89% and 42% of MB were removed at MB concentrations
272 equal to 5, 10 and 20 mg/L, respectively. The HTNF removed almost all the dye at relatively
273 low initial concentration. In industrial applications, high MB removal at low concentrations is
274 considered to be of a great importance. The amount of MB adsorbed increased with time until
275 the equilibrium was attained at 30 min for high MB concentrations (10 and 20 mg/L), while
276 almost all MB molecules were adsorbed within 5 min at 5 mg/L of MB. The initial uptake
277 (first few minutes) for MB was high because a large number of adsorption sites were
278 available for adsorption. Later on, the adsorption decreased as the repulsive forces between
279 the adsorbed MB molecules (on HTNF) and the MB molecules in the solution increased
280 (Fetterolf et al., 2003; Xiong et al., 2010). In order to study the effect of other parameters in
281 the adsorption process such as pH and temperature, 20 mg/L MB concentration was selected
282 and will be discussed in the following sections.

283

284 **Figure 5**

285

286 3.1.2.3. Effect of Solution pH

287

288 The adsorption of MB was studied in a suspension of 0.5 g/L of HTNF and 20 mg/L of MB
289 using different pH values (3, 5, 7 and 9). The results of adsorption are shown in Figure 6. MB
290 is a cationic dye which is favourably adsorbed on negatively charged surfaces (Fetterolf et al.,
291 2003). The zeta potential measurements of HTNF revealed that the surface charge of the
292 nanofibres was negative over a wide pH range, and that the PZC was around pH 3.2. At pH 3,
293 the repulsive forces between the HTNF and MB molecules dominated the adsorption process,
294 leading to a low overall adsorption (7% after 30 min). In contrast, when the pH was increased
295 to 5, 7, and 9, MB adsorption increased to 28%, 32% and 42%, respectively. This was mainly
296 due to electrostatic attraction between the HTNF surface and MB molecules. This finding
297 was in agreement with previous studies on the adsorption of MB onto titania (Fetterolf et al.,
298 2003), titanate nanotubes (Xiong et al., 2010) and different organic and inorganic adsorbent
299 (Ai et al., 2011).

300

301 **Figure 6**

302

303 3.1.2.4. Effect of Solution Temperature

304

305 The effect of different solution temperatures on the adsorption is shown in Figure 7. The
306 adsorption of MB increased with temperature increase, indicating an endothermic adsorption
307 process (Bulut and Aydin, 2006; Hong et al., 2009). The total adsorption at equilibrium (30
308 min) was found to increase from 42% to 52% for an increase in the solution temperatures
309 from 25 to 45 °C.

310

311 **Figure 7**

312

313 3.1.2.5. Adsorption Equilibrium and Isotherms

314

315 Figures 8A and 8B show the amount of MB adsorbed at equilibrium (30 min) using different
316 HTNF loadings and MB concentrations, respectively. The adsorption of dye increased with
317 HTNF loading to a maximum of 17.8 mg/g at 0.5 g/L and then decreased to 9.18 and 4.64
318 mg/g at 1 and 2 g/L, respectively. The increase in the adsorption capacity (q_e) reached a
319 maximum at 0.5 g/L of HTNF loading while further increase in the mass of HTNF
320 (denominator in Eq.2) with $(C_0 - C_e) * V$ (Eq. 1) remaining constant caused the decrease in q_e .

321 The effect of initial MB concentration revealed that the increase of MB concentration at a
322 constant HTNF loading increased the adsorption mainly because of high driving force for
323 mass transfer (Bulut and Aydin, 2006). The data plotted in Figure 8B showed some decrease
324 in q_e after increasing the concentration of MB from 10 to 20 mg/L (data collected after 30
325 min of contact). However, the experiments were continued for 3 h and no significant
326 difference in q_e at MB concentrations of 10 mg/L and 20 mg/L was found (q_e for both
327 concentrations varied from 16.5 to 17.8 mg/g).

328

329 **Figure 8**

330

331 During adsorption, the adsorption capacity is highly influenced by the pH variations of the
332 solution (Wang et al., 2005). The plot of pH variation against the adsorption capacity is
333 shown in Figure 9A. The adsorption capacity increased from 2.55 mg/g at pH 3 to 16.57
334 mg/g at pH 9 after 30 min of contact. As discussed earlier, the surface charge of HTNF
335 changed from positive to negative at pH 3 and 9, respectively. This played an important role
336 in adsorbing more cationic MB molecule at high pH.

337

338 Increasing the temperature of the solution enhanced the adsorption of MB molecules onto
339 HTNF (Figure 9B). The adsorption capacity increased from 16.57 mg/g at 25 °C to 19 mg/g
340 at 45 °C. It has been discussed earlier in this study that the process of adsorption is
341 endothermic. The heat of adsorption can describe the physical or chemical adsorption of gas
342 molecules into solid surfaces (Sircar, 2005). Nevertheless, the use of endothermic and
343 exothermic adsorption terminologies to explain adsorption in water has been widely accepted.

344

345 To further describe the equilibrium of adsorption, the most commonly used adsorption model
346 (Langmuir) has been used to fit the data obtained under different operating conditions. The
347 data was fitted using Eq. 3 and the results are shown in Table 1. Our data fitted well the
348 Langmuir model. The goodness of fit was shown with R^2 equal to 0.99, 0.91, 0.89 and 0.99
349 for experiments on HTNF loading, MB concentration, pH and temperature, respectively.
350 These findings indicated that the monolayer adsorption of MB on HTNF was the dominant
351 mechanism of adsorption. The Langmuir model has fitted well the adsorption data of MB
352 onto titanate nanotubes (Xiong et al., 2010). It has been reported that uniform nanotubular
353 structure and homogenous distribution of active sites on the walls favoured this adsorption
354 mechanism.

355

356 **Figure 9**

357

358 **Table 1**

359

360 The Langmuir isotherm was further evaluated by the dimensionless constant separation factor
361 R_L (Hall et al., 1966; Weber and Chakravorti, 1974):

362

$$363 \quad R_L = \frac{1}{1+kC_0} \quad (\text{Eq. 5})$$

364

365 With k Langmuir constant (L/mg) and C_0 initial MB concentration (mg/L). The value of R_L
366 indicates the shape of the adsorption isotherm and values between 0 and 1 indicate favourable
367 adsorption (McKay et al., 1982). The calculated R_L from our data showed values between 0
368 and 1 suggesting that the adsorption between MB and HTNF was favourable (Table 2).
369 Moreover, low R_L values (<0.04) indicated that the interaction between MB and HTNF was
370 relatively strong (Xiong et al., 2010).

371

372 **3.1.3. Photocatalytic Decolourisation and DOC Removal of MB**

373 3.1.3.1. Effect of Solution pH

374

375 The variation of solution pH directly influenced the adsorption of MB molecules onto HTNF
376 through electrostatic interactions. The adsorption was favoured at high pH between different
377 surface charges and decreased with pH decrease. Figure 10 shows the discolouration and the
378 DOC removal of MB solution after 30 min adsorption and 180 min of light irradiation. The
379 discolouration of the solution was almost complete after 90 min for pH values of 5, 7 and 9.
380 In contrast, only 89% of MB was removed after 180 min of light irradiation at pH 3. The
381 decrease in DOC was slower being 48%, 75%, 78% and 78% for pHs of 3, 5, 7 and 9. The
382 results of regression analysis between MB discolouration and DOC removal are presented in
383 Table 3.

384

385 The effect of solution pH on the discolouration of MB solution was reported in the literature
386 (Shimizu et al., 2007; Tayade et al., 2009). Shimizu et al. (2007) found that the change of pH
387 between 3 and 10 did not influence the solution colour in the absence of the photocatalyst.

388 However, significant decrease in colour was reported at pH above 10. In this study, the pH
389 range was between 3 and 9, thus it can be assumed that the initial concentration of MB was
390 constant. Moreover, photodegradation data collected in different experiments were
391 normalised to the initial MB absorbance measured at pH values of 3, 5, 7 and 9. Lachheb et
392 al. (2002) studied the adsorption of several dyes, including MB, onto TiO₂ under different pH
393 values ranging from 3 to 9. In agreement with the present findings, they also reported low
394 MB adsorption at low pH but little influence of pH variations upon the kinetics of colour
395 disappearance under UV light. In another study on MB photodegradation, Wu and Chern
396 (2006) showed that increasing the pH above the PZC of TiO₂ (PZC \approx 4.5 according to
397 authors' measurements) has dramatically impacted the dispersion of particles in solution,
398 leading to coagulation and sedimentation. Consequently, the decomposition of MB was
399 decreased because of the decrease in TiO₂ surface area. In this study, no coagulation of
400 HTNF was observed but the decrease of adsorption (at pH 3) retarded the discolouration.
401 This observation indicates that the decomposition of MB molecules was due to the attack by
402 the OH[•] radicals near the HTNF surface under these conditions. In contrast, surface
403 degradation was the dominating degradation mechanism at high solution pH.

404

405 **Figure 10**

406

407 **Table 3**

408

409 3.1.3.2. Effect of Light Intensity

410

411 The effect of light intensity on the photodegradation of MB was studied and the results are
412 shown in Figure 11. The light intensity of the system can affect the electron/hole formation,
413 their separation and recombination rate. However, this can also be affected by the emitted
414 wavelength of the lamp and the type of photocatalyst. In the reactor used in the present
415 experiments, the decrease of light intensity from 28000 lx to 15000 lx did not significantly
416 decrease the degradation rate of MB after 180 min of light irradiation. However, a further
417 reduction in light intensity to 5000 lx resulted in 25% decrease in discolouration efficiency of
418 the system (adsorption + photodegradation). DOC removal of the system was high (78%) for
419 the maximum intensity (28000 lx), decreasing to 73% at 15000 lx and to 64% at 5000 lx.

420

421 The pseudo-first order apparent constants are shown in Table 4. These were calculated by
422 using the decrease in MB concentration (k^l_a) and the decrease of solution DOC (k^2_a) over
423 time. k^l_a values increased from 0.011 min⁻¹ at pH 3 to 0.034 min⁻¹ at pH 9. Similarly, k^l_a
424 increased from 0.0037 min⁻¹ to 0.034 min⁻¹ with the increase in light intensity. The
425 photodiscolouration of MB over HTNF followed the pseudo-first order reaction kinetics,
426 noting that similar finding was reported by Houas et al. (2001) for photodegrading MB over
427 Degussa P25.

428

429 **Figure 11**

430

431 k^2_a was calculated from the DOC concentration decrease over time (Table 4). DOC removal
432 kinetics were slower than those observed for MB discolouration and this could be attributed
433 to the formation of photodegradation intermediates (Herrmann, 1999; Houas et al., 2001;
434 Lachheb et al., 2002). The apparent rate constant increased with pH and light intensity
435 increase. The adsorption of MB onto HTNF favoured its photocatalytic removal from the
436 solution at basic pH (Houas et al., 2001).

437

438 **Table 4**

439

440 **3.1.4. Photocatalytic Stability of HTNF**

441

442 The photocatalytic stability of HTNF was also tested by adopting the experimental model of
443 Xiong et al. (2011). The experiments consisted of running photocatalytic degradation
444 reactions without the dark adsorption of MB onto HTNF. A 200 mL beaker containing 0.1 g
445 of HTNF suspended in 20 mg/L MB solution was placed in the solar simulator at 28000 lx
446 and at a temperature of 26 °C.

447

448 Figures 12 and 13 show the normalised photocatalytic degradation data obtained from the
449 absorbances at $\lambda = 254$ nm and 664 nm. The MB solution changed to colourless after 2 h of
450 photoreaction, then turned to humic-like water colour between 2 h to 6 h before becoming
451 colourless at the end (after almost 8 h). These findings suggest that the photocatalytic
452 degradation of MB in this system has occurred in three stages:

- 453 • Stage 1: Concurrent adsorption of MB and photocatalytic degradation to
454 positively charged intermediates (surface reaction) (Houas et al., 2001; Orendorz
455 et al., 2008).
- 456 • Stage 2: Desorption of intermediate compounds, (mainly negatively charged
457 phenolic or aromatic organics) from HTNF surface (Houas et al., 2001).
- 458 • Stage 3: Degradation of aromatic intermediates by OH^\bullet attacks.

459

460 The experiments were repeated using the recycled photocatalyst over three degradation
461 cycles, with no significant changes in photocatalytic activity (Figure 14).

462

463 **Figure 12**

464

465 **Figure 13**

466

467 **Figure 14**

468

469 **3.1.5. Settling Characteristic of HTNF**

470

471 The high cost associated with the separation of titania at commercial scale has seriously
472 retarded the use of industrial photocatalysis. At the end of photocatalysis, the facile recovery
473 of the photocatalyst is very important for its reuse. A low cost catalyst separation process can
474 be achieved by settling of particles. Accordingly, the settling characteristics of HTNF were
475 also evaluated by comparing the sedimentation of HTNF to Degussa P25 in aqueous
476 suspensions (Figure 15). The catalyst concentration was 0.5 g/L at a pH of 9. Rapid HTNF
477 sedimentation was recorded by measuring the turbidity of decanted solution at fixed time
478 intervals. About 80% turbidity removal was achieved after 30 min of settling that increased
479 up to 90% after 2 h settling time. In contrast, the turbidity of P25 suspension did not change
480 significantly. In a similar study, Xiong et al. (2011) reported 72% decrease in turbidity within
481 180 min settling time for titanate nanotubes (0.5 g/L titanate loading in a 300 mL square
482 photoreactor). The rapid sedimentation of HTNF is another advantage for their industrial
483 application in wastewater photocatalysis.

484

485 **Figure 15**

486
487
488
489
490
491
492
493
494
495
496
497
498
499
500
501
502
503
504
505
506
507
508
509
510
511
512
513
514
515
516
517
518
519

4. Conclusions

H-titanate nanofibres were synthesised by an aqueous peroxide route at high pH. The HTNF were characterised for changes in morphology by observing SEM images which revealed randomly dispersed nanofibres with an average diameter of 40-70 nm and few hundred nanometers in length. The nanofibres were negatively charged over a wide pH range and their PZC was found at pH 3.2. H^+ successfully replaced Na^+ in the nanofibres by ion exchange as confirmed by EDS measurements. The HTNF were mainly anatase with a surface area of $31.54 \text{ m}^2/\text{g}$, average pore volume of $0.10 \text{ cm}^3/\text{g}$ and average pore size of 50 \AA .

The adsorption of MB onto HTNF was examined by investigating the effect of HTNF loading, MB concentration, solution pH, and temperature on the adsorption capacity. The results showed that the adsorption of MB was promoted by high catalyst loadings, high pH (greater than the PZC) and temperature. The adsorption capacity increased from 2.55 mg/g at pH 3 to 16.57 mg/g at pH 9 after 30 min of contact, and from 16.57 mg/g at $25 \text{ }^\circ\text{C}$ to 19 mg/g at $45 \text{ }^\circ\text{C}$. The adsorption data fitted well the Langmuir model for all operational conditions. The optimum operational conditions for the adsorption of MB onto HTNF were found at 0.5 g/L of photocatalyst, 10 mg/L MB, pH 9 and temperature of $45 \text{ }^\circ\text{C}$.

The photocatalytic degradation of MB was studied under simulated solar light to study the effect of pH and light intensity. No significant differences were found for the discolouration of MB at pHs greater than the PZC. However, at pH 3, the decrease in MB adsorption significantly reduced its consecutive photocatalytic degradation. The increase in light intensity from 5000 lx to 28000 lx was found to increase 10 folds the discolouration of MB, according to the apparent degradation constant (k^1_a) obtained from the L-H model. In contrast, the DOC removal at the highest light intensity was only twice as good as the DOC removal found at the lowest light intensity (k^2_a).

The photocatalytic activity of the nanofibres was found stable after 3 degradation cycles using the adsorption/photocatalysis model. Moreover, the fibres were easily separated from the solution by settling at room temperature.

520

521

522 **Acknowledgment**

523 This research was funded by ARC-LP, a UTS internal grant and Australian Postgraduate
524 Award scholarship. This work was supported by Priority Research Centers Program through
525 the National Research Foundation of Korea (NRF) funded by the Ministry of Education,
526 Science and Technology (2009-0094055).

527

528 **References**

529

530 Ai, L., Li, M., Li, L., 2011. Adsorption of methylene blue from aqueous solution with
531 activated carbon/cobalt ferrite/alginate composite beads: kinetics, isotherms, and
532 thermodynamics. *Journal of Chemical and Engineering Data* 56(8), 3475-3483.

533 Baiju, K.V., Shukla, S., Biju, S., Reddy, M.L.P., Warriar, K.G.K., 2009. Hydrothermal
534 processing of dye-adsorbing one-dimensional hydrogen titanate. *Materials Letters*
535 63(11), 923-926.

536 Bela, S., Wong, A.S.W. and Ho., G.W., 2010. Hydrolysis and ion exchange of titania
537 nanoparticles towards large-scale titania and titanate nanobelts for gas sensing
538 applications. *Journal of Physics D: Applied Physics* 43(3), 035401.

539 Bulut, Y., Aydin, H., 2006. A kinetics and thermodynamics study of methylene blue
540 adsorption on wheat shells. *Desalination* 194, 259-267.

541 El Saliby, I., Erdei, L., Shon, H.K., Kim, J.B., Kim, J.-H., 2011a. Preparation and
542 characterisation of mesoporous photoactive Na-titanate microspheres. *Catalysis*
543 *Today* 164(1), 370-376.

544 El Saliby, I., Shon, H.K., Kandasamy, J., Kim, J.-H., 2011b. Synthesis, characterisation and
545 separation of photoreactive Hydrogen-titanate nanofibrous channel. *Separation*
546 *Purification Technology* 77(2), 202-207.

547 Fetterolf, M.L., Patel, H.V., Jennings, J.M., 2003. Adsorption of methylene blue and acid
548 blue 40 on titania from aqueous solution. *Journal of Chemical and Engineering Data*
549 48(4), 831-835.

550 Hall, K.R., Eagleton, L.C., Acrivos, A., Vermeulen, T., 1966. Pore- and solid-diffusion
551 kinetics in fixed-bed adsorption under constant-pattern conditions. *Industrial and*
552 *Engineering Chemistry Fundamentals* 5(2), 212-223.

553 Herrmann, J.-M., 1999. Heterogeneous photocatalysis: fundamentals and applications to the
554 removal of various types of aqueous pollutants. *Catalysis Today* 53(1), 115-129.

555 Hong, S., Wen, C., He, J., Gan, F. and Ho, Y.-S., 2009. Adsorption thermodynamics of
556 methylene blue onto bentonite. *Journal of Hazardous Materials* 167, 630-633.

557 Houas, A., Lachheb, H., Ksibi, M., Elaloui, E., Guillard, C., Herrmann, J.-M., 2001.
558 Photocatalytic degradation pathway of methylene blue in water. *Applied Catalysis B:*
559 *Environmental* 31(2), 145-157.

560 Lachheb, H., Puzenat, E., Houas, A., Ksibi, M., Elaloui, E., Guillard, C., Herrmann, J.-M.,
561 2002. Photocatalytic degradation of various types of dyes (Alizarin S, Crocein Orange
562 G, Methyl Red, Congo Red, Methylene Blue) in water by UV-irradiated titania.
563 *Applied Catalysis B: Environmental* 39(1), 75-90.

564 Langmuir, I., 1918. The adsorption of gases on plane surfaces of glass, mica and platinum.
565 *Journal of the American Chemical Society* 40(9), 1361-1403.

566 Lee, C.-K., Lin, K.-S., Wu, C.-F., Lyu, M.-D., Lo, C.-C., 2008a. Effects of synthesis
567 temperature on the microstructures and basic dyes adsorption of titanate nanotubes.
568 *Journal of Hazardous Materials* 150(3), 494-503.

569 Lee, C.-K., Liu, S.-S., Juang, L.-C., Wang, C.-C., Lyu, M.-D., Hung, S.-H., 2007.
570 Application of titanate nanotubes for dyes adsorptive removal from aqueous solution.
571 *Journal of Hazardous Materials* 148(3), 756-760.

572 Lee, C.-K., Wang, C.-C., Juang, L.-C., Lyu, M.-D., Hung, S.-H., Liu, S.-S., 2008b. Effects of
573 sodium content on the microstructures and basic dye cation exchange of titanate
574 nanotubes. *Colloids and Surfaces A: Physicochemical and Engineering Aspects* 317,
575 164-173.

576 Mao, Y., Kanungo, M., Hemraj-Benny, T., Wong, S.S., 2006. Synthesis and growth
577 mechanism of titanate and titania one-dimensional nanostructures self-assembled into
578 hollow micrometer-scale spherical aggregates. *The Journal of Physical Chemistry B*
579 110(2), 702-710.

580 McKay, G., Blair, H.S., Gardner, J.R., 1982. Adsorption of dyes on chitin. I. Equilibrium
581 studies. *Journal of Applied Polymer Science* 27(8), 3043-3057.

582 Nyman, M., Hobbs, D.T., 2006. A Family of Peroxo-titanate Materials Tailored for Optimal
583 Strontium and Actinide Sorption. *Chemistry of Materials* 18(26), 6425-6435.

584 Orendorz, A., Ziegler, C., Gnaser, H., 2008. Photocatalytic decomposition of methylene blue
585 and 4-chlorophenol on nanocrystalline TiO₂ films under UV illumination: A ToF-
586 SIMS study. *Applied Surface Science* 255(4), 1011-1014.

587 Sircar, S. (2005) Heat of adsorption on heterogeneous adsorbents. *Applied Surface Science*
588 252(3), 647-653.

589 Shimizu, N., Ogino, C., Dadjour, M.F., Murata, T., 2007. Sonocatalytic degradation of
590 methylene blue with TiO₂ pellets in water. *Ultrasonics Sonochemistry* 14(2), 184-190.

591 Tayade, R.J., Natarajan, T.S., Bajaj, H.C., 2009. Photocatalytic degradation of methylene
592 blue dye using ultraviolet light emitting diodes. *Industrial and Engineering Chemistry*
593 *Research* 48(23), 10262-10267.

594 Wang, S., Boyjoo, Y., Choueib, A., 2005. A comparative study of dye removal using fly ash
595 treated by different methods. *Chemosphere* 60(10), 1401-1407.

596 Weber, T.W., Chakravorti, R.K., 1974. Pore and solid diffusion models for fixed-bed
597 adsorbents. *AIChE Journal* 20(2), 228-238.

598 Wei, M., Konishi, Y., Zhou, H., Sugihara, H., Arakawa, H., 2004. A simple method to
599 synthesize nanowires titanium dioxide from layered titanate particles. *Chemical*
600 *Physics Letters* 400, 231-234.

601 Wu, C.-H., Chern, J.-M., 2006. Kinetics of photocatalytic decomposition of methylene blue.
602 *Industrial and Engineering Chemistry Research* 45(19), 6450-6457.

603 Xiong, L., Sun, W., Yang, Y., Chen, C., Ni, J., 2011. Heterogeneous photocatalysis of
604 methylene blue over titanate nanotubes: Effect of adsorption. *Journal of Colloid and*
605 *Interface Science* 356(1), 211-216.

606 Xiong, L., Yang, Y., Mai, J., Sun, W., Zhang, C., Wei, D., Chen, Q., Ni, J., 2010. Adsorption
607 behavior of methylene blue onto titanate nanotubes. *Chemical Engineering Journal*
608 156(2), 313-320.

609 Zhu, H., Gao, X., Lan, Y., Song, D., Xi, Y., Zhao, J., 2004. Hydrogen titanate nanofibers
610 covered with anatase nanocrystals: A delicate structure achieved by the wet chemistry
611 reaction of the titanate nanofibers. *Journal of the American Chemical Society*
612 126(27), 8380-8381.

613

614 **List of Figures**

615

616 **Figure 1.** Zeta potential of 1 g/L suspension of as-prepared (AP-HTNF) and calcined HTNF
617 (C-HTNF).

618 **Figure 2.** SEM images of H titanate nanofibres (A and B).

619 **Figure 3.** EDS plot showing the elemental composition of HTNF.

620 **Figure 4.** Effect of HTNF loading on the adsorption of MB from solution. (Experimental
621 conditions: MB = 10 mg/L, T = 25 °C, shaking speed = 150 rpm, pH = 9).

622 **Figure 5.** Effect of initial MB concentration on the adsorption of MB onto HTNF.
623 (Experimental conditions: HTNF = 0.5 g/L, T = 25 °C, shaking speed = 150 rpm, pH = 9).

624 **Figure 6.** Effect of solution pH on the adsorption of MB onto HTNF. (Experimental
625 conditions: HTNF = 0.5 g/L, MB = 20 mg/L, T = 25 °C, shaking speed = 150 rpm).

626 **Figure 7.** Effect of solution temperature on the adsorption of MB onto HTNF. (Experimental
627 conditions: HTNF = 0.5 g/L, MB = 20 mg/L, shaking speed = 150 rpm, pH = 9).

628 **Figure 8.** (A) Effect of HTNF loading and (B) MB concentration on the amount of dye
629 adsorbed at equilibrium (q_e , mg/g) (Experimental conditions: T = 25 °C, shaking speed = 150
630 rpm, pH = 9).

631 **Figure 9.** (A) Effect of solution's pH and (B) temperature on the amount of dye adsorbed at
632 equilibrium (q_e , mg/g) (Experimental conditions: HTNF = 0.5 g/L, MB = 20 mg/L, shaking
633 speed = 150 rpm).

634 **Figure 10.** (A) Effect of solution pH on the discolouration and (B) DOC removal of MB
635 solution using HTNF. (Experimental conditions: HTNF = 0.5 g/L, MB = 20 mg/L, T = 26 °C,
636 air flow = 0.6 L/min, light intensity = 28 000 lx).

637 **Figure 11.** Effect of light intensity on the discolouration (A) and DOC removal (B) of MB
638 solution using HTNF. (Experimental conditions: HTNF = 0.5 g/L, MB = 20 mg/L, T = 26 °C,
639 air flow = 0.6 L/min, pH = 9).

640 **Figure 12.** (A) Photocatalytic degradation of MB, (B) desorption of intermediate products
641 and (C) Photocatalytic decomposition of intermediates ("NA" stands for normalised
642 absorbance).

643 **Figure 13.** UV-vis spectrum for the photocatalytic degradation of MB showing three stages
644 (stage 1: 0 to 120 min; stage 2: 121 to 360 min; stage 3: 361 to 480 min).

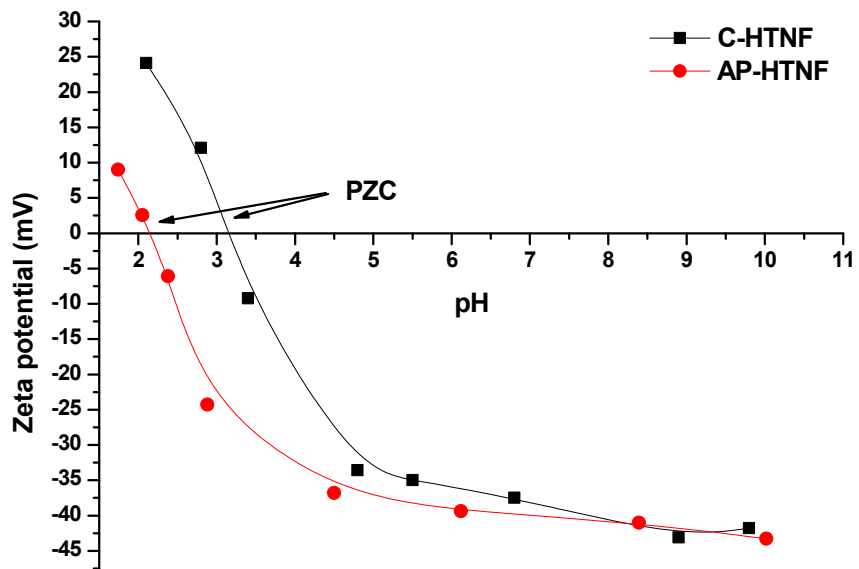
645 **Figure 14.** Photocatalytic stability of HTNF over three degradation cycles.

646 **Figure 15.** Normalised turbidity decrease in function of sedimentation time for HTNF and
647 Degussa P25.

648 **Figure 1**

649

650



651

652

653

654

655

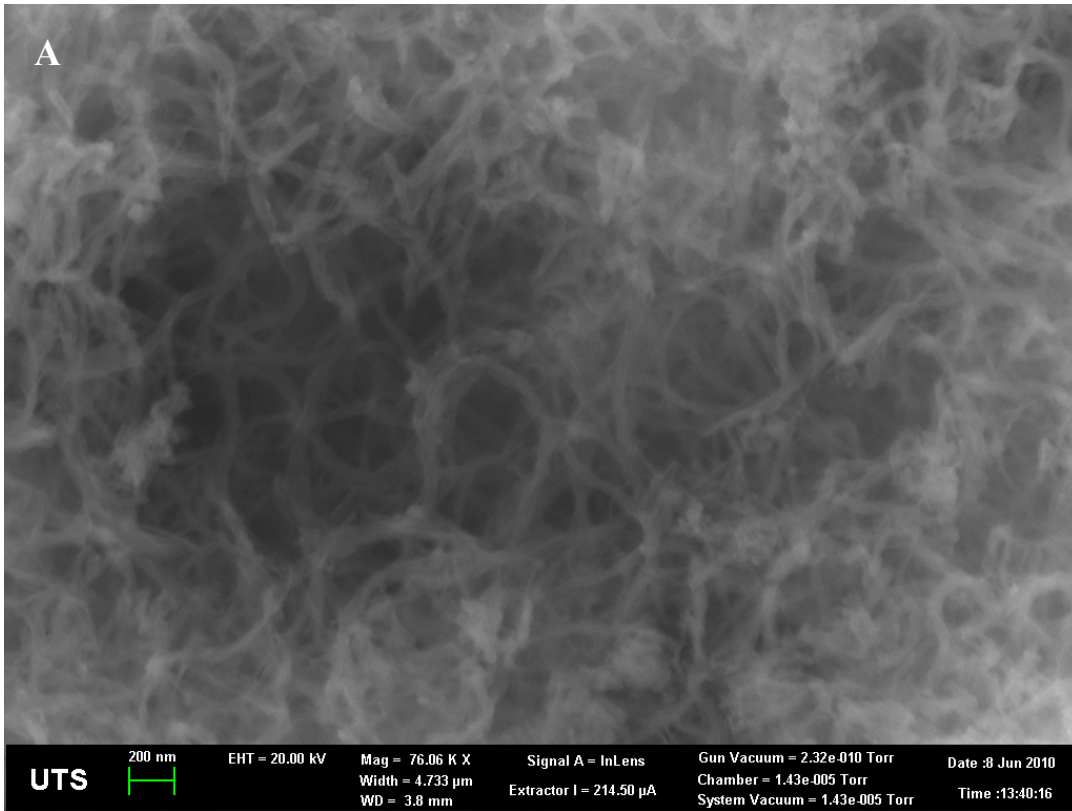
656

657

658

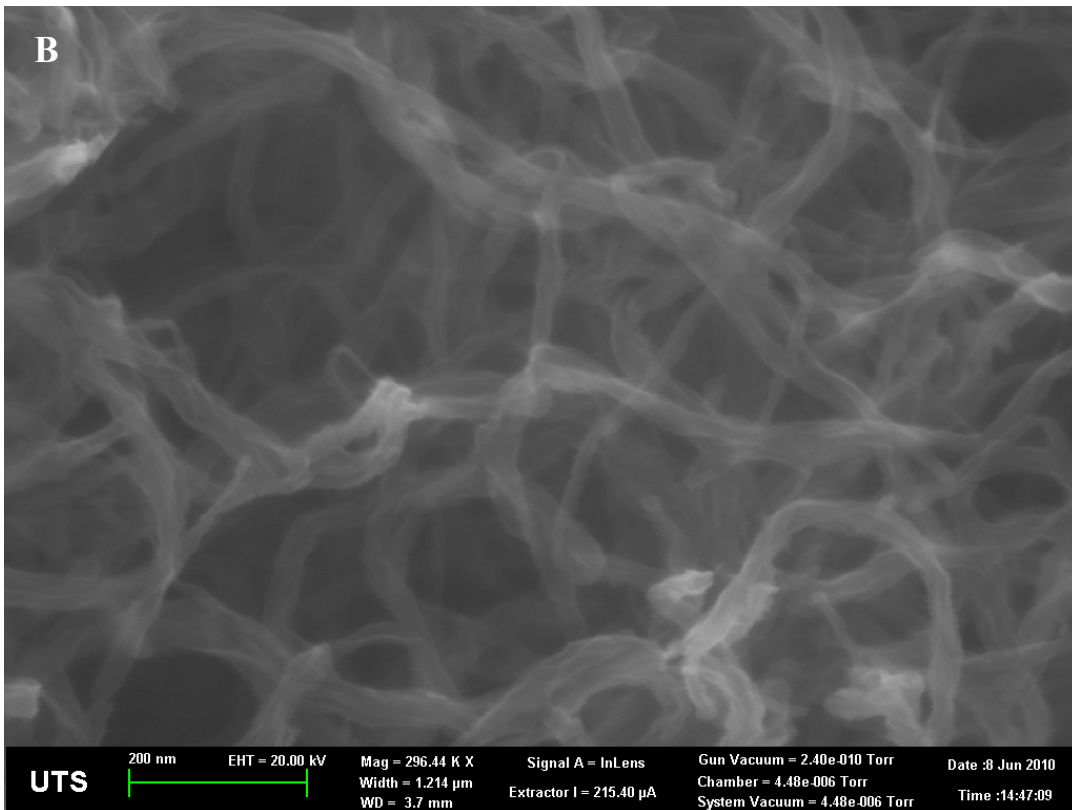
659 **Figure 2**

660



661

662



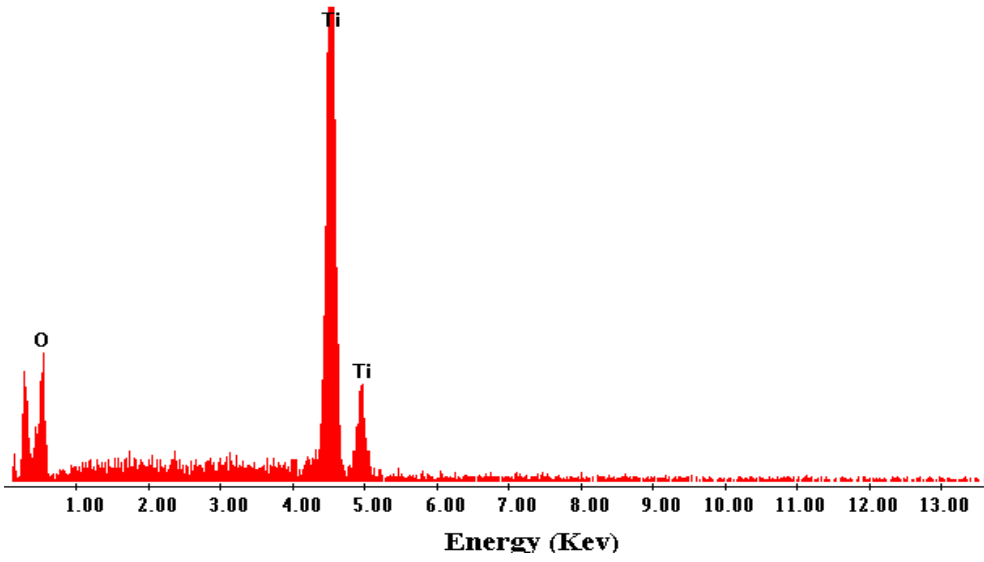
663

664

665 **Figure 3**

666

HTNF



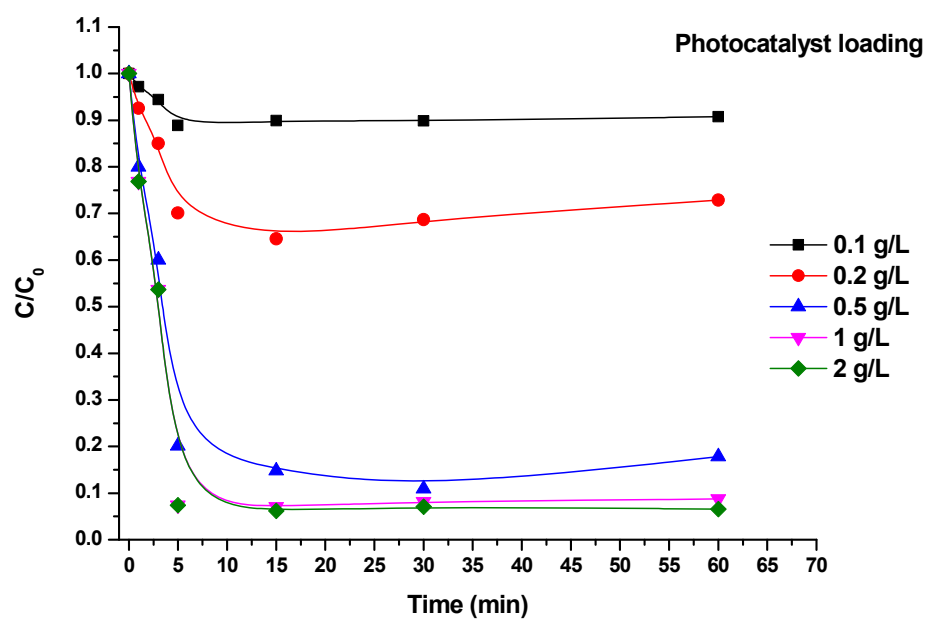
667

668

669

670 **Figure 4**

671

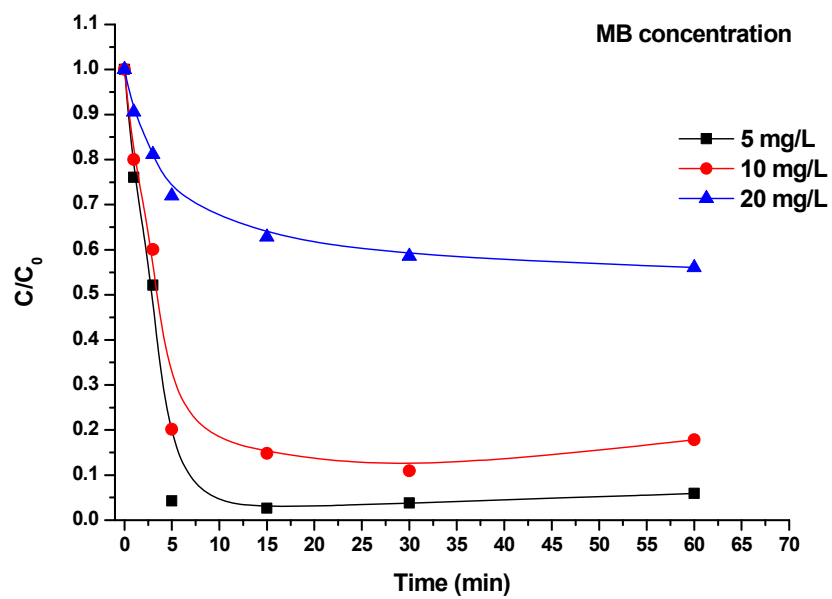


672

673

674 **Figure 5**

675

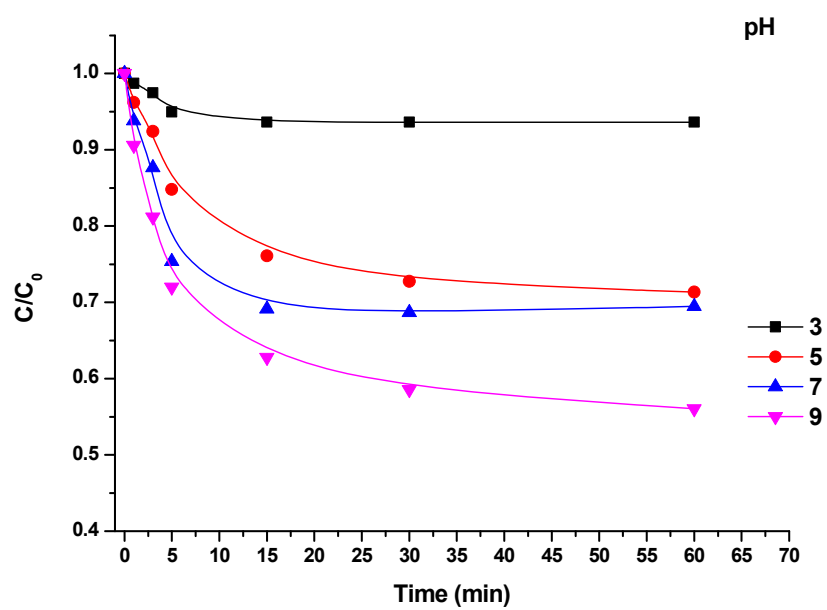


676

677

678 **Figure 6**

679

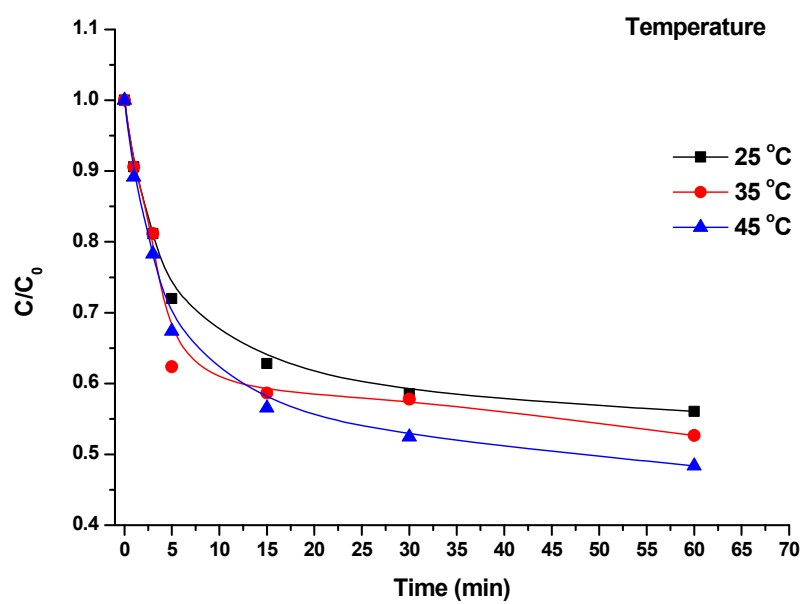


680

681

682 **Figure 7**

683

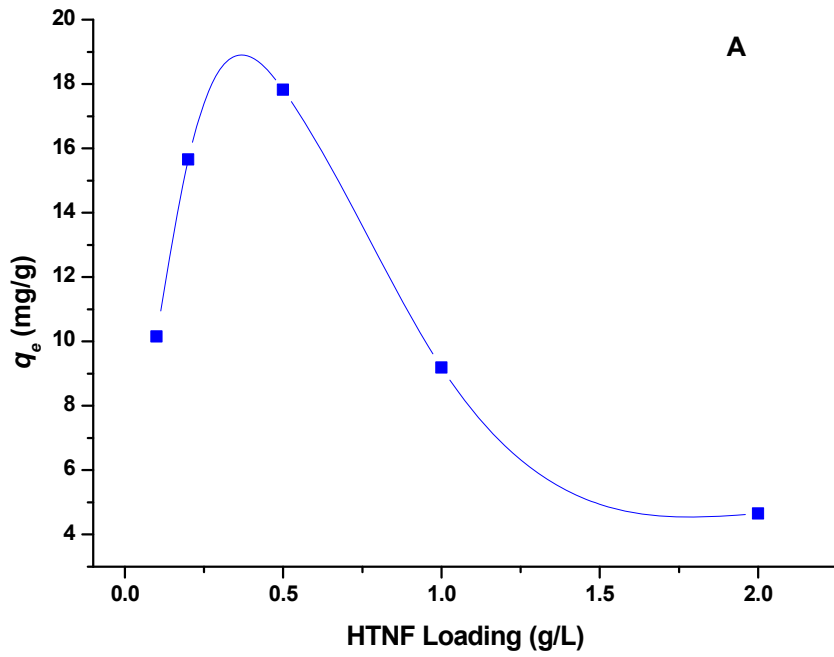


684

685

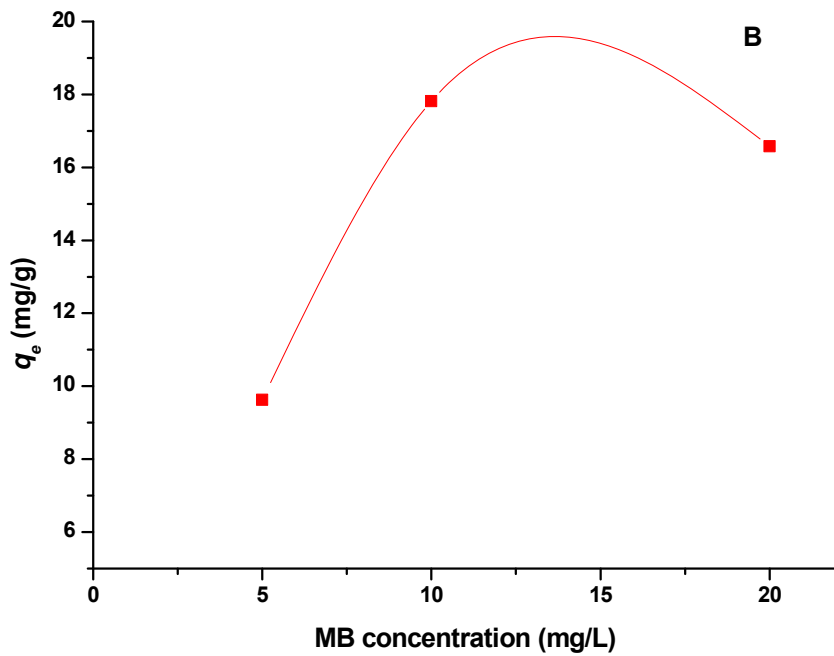
686 **Figure 8**

687



688

689

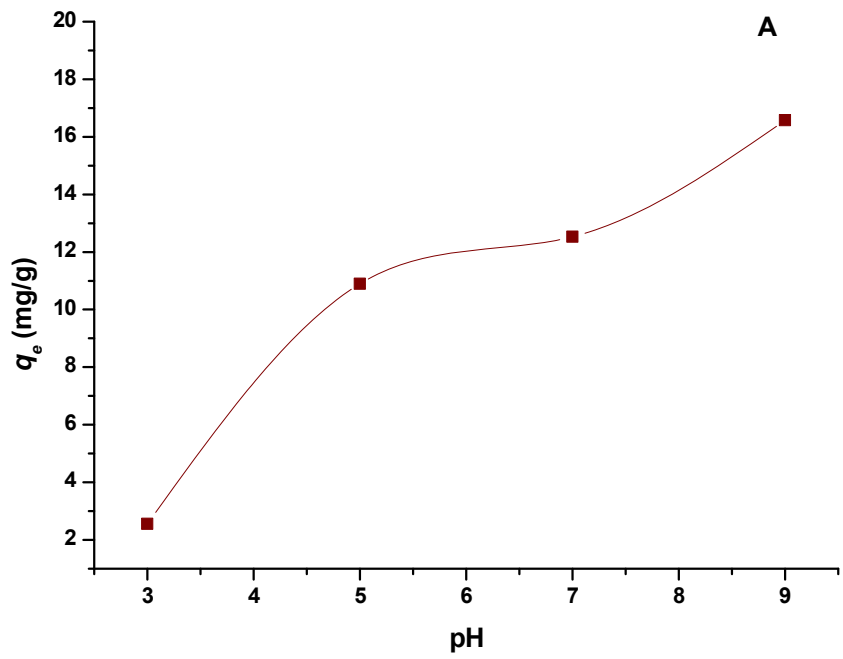


690

691

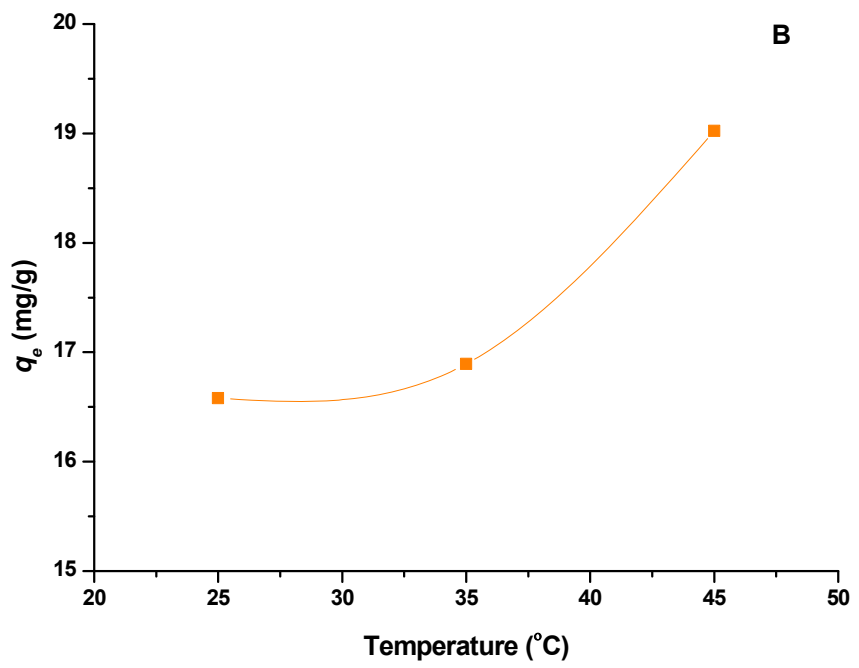
692 **Figure 9**

693



694

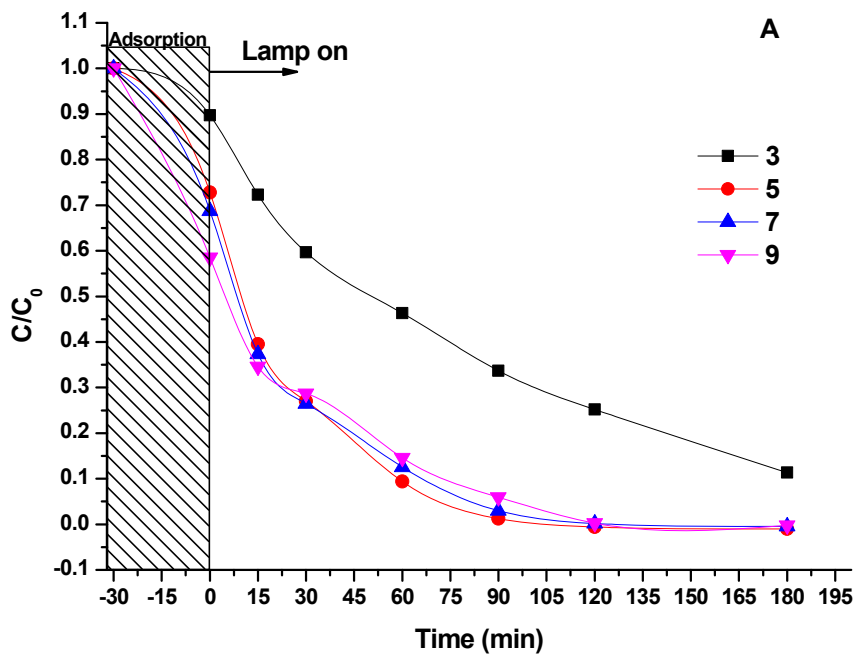
695



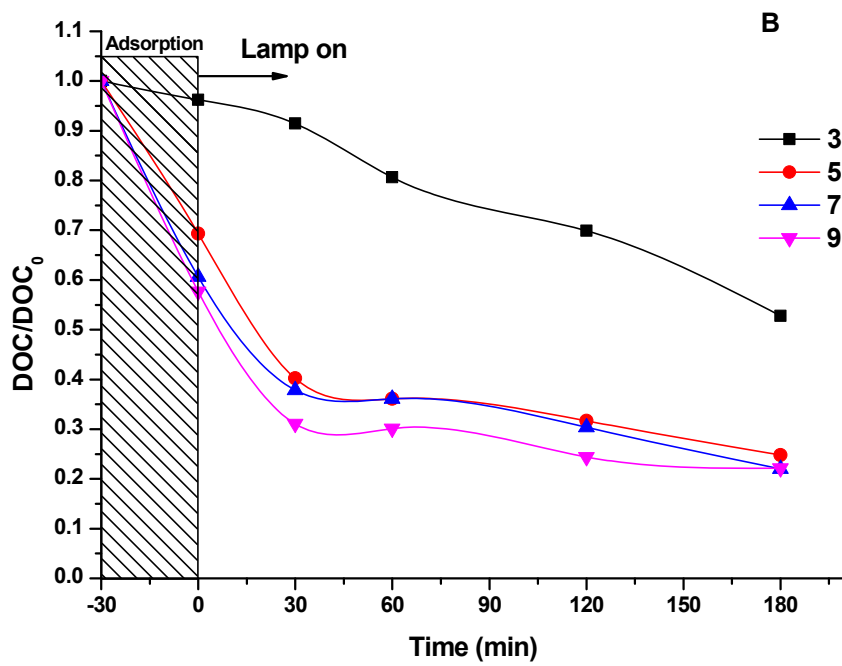
696

697

698 **Figure 10**
699



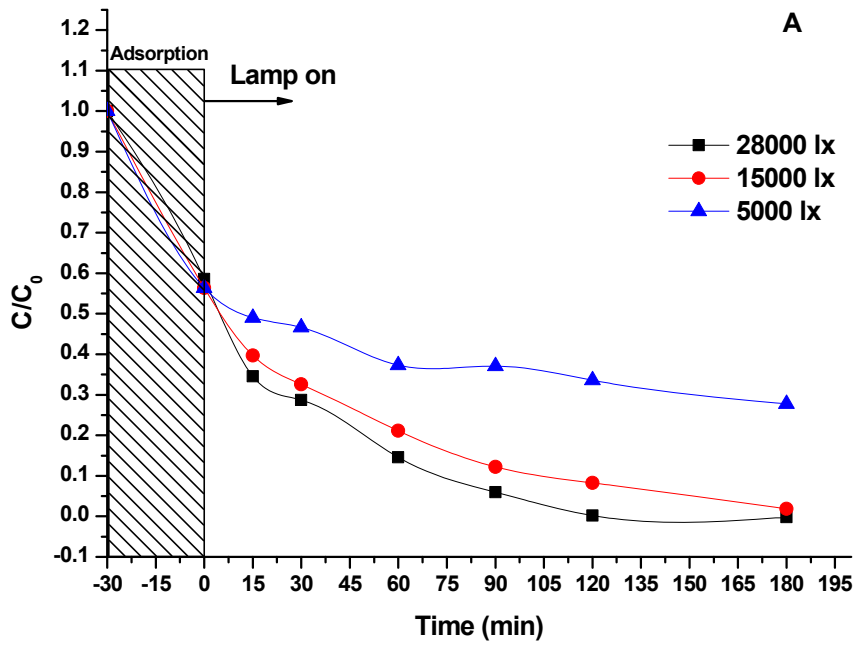
700



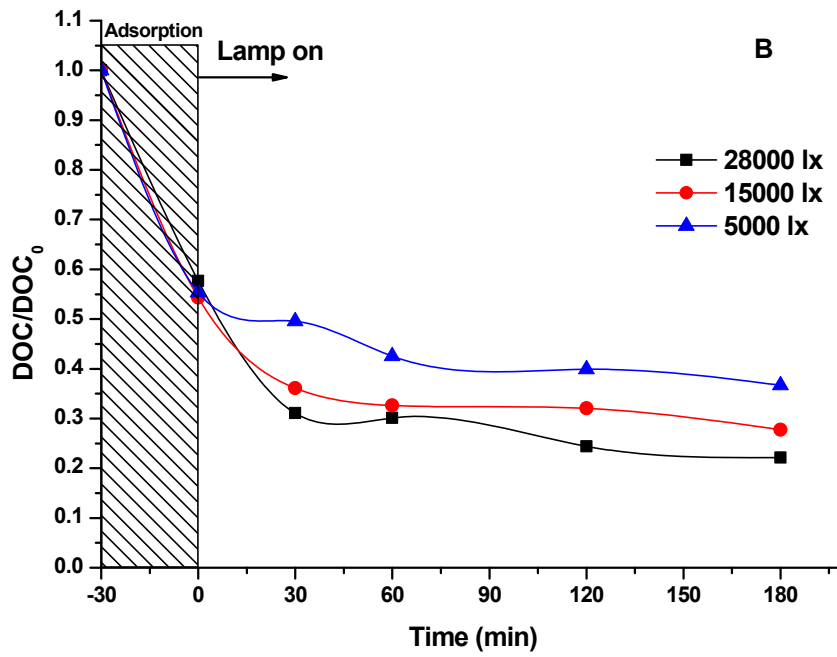
701

702

703 **Figure 11**
704



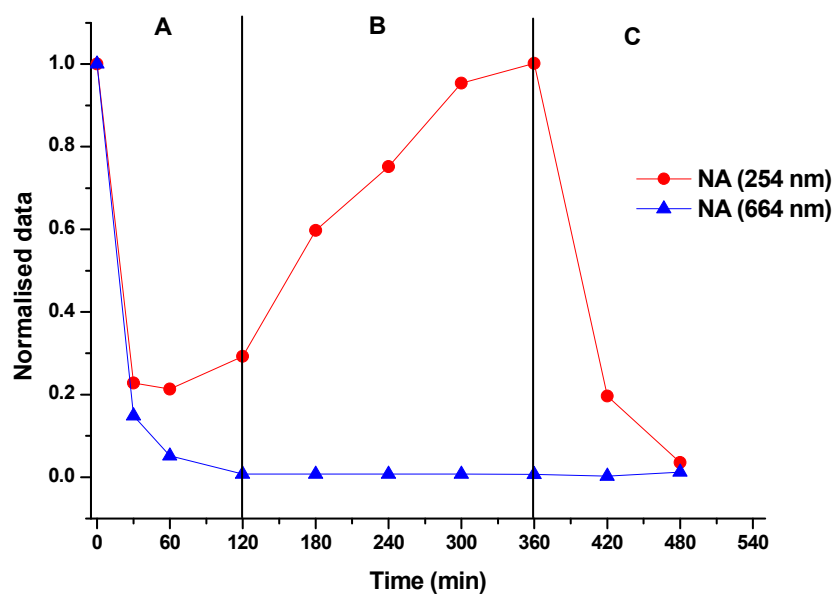
705



706

707

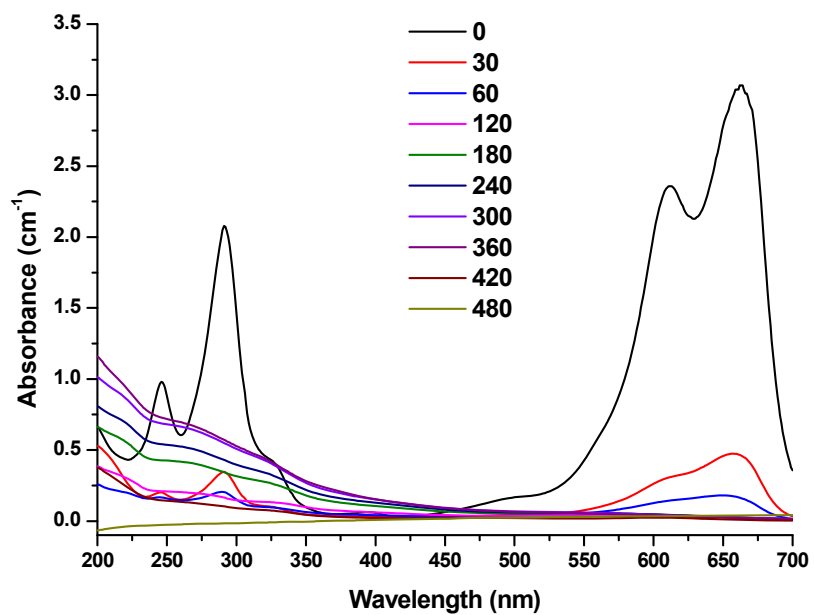
708 **Figure 12**



709

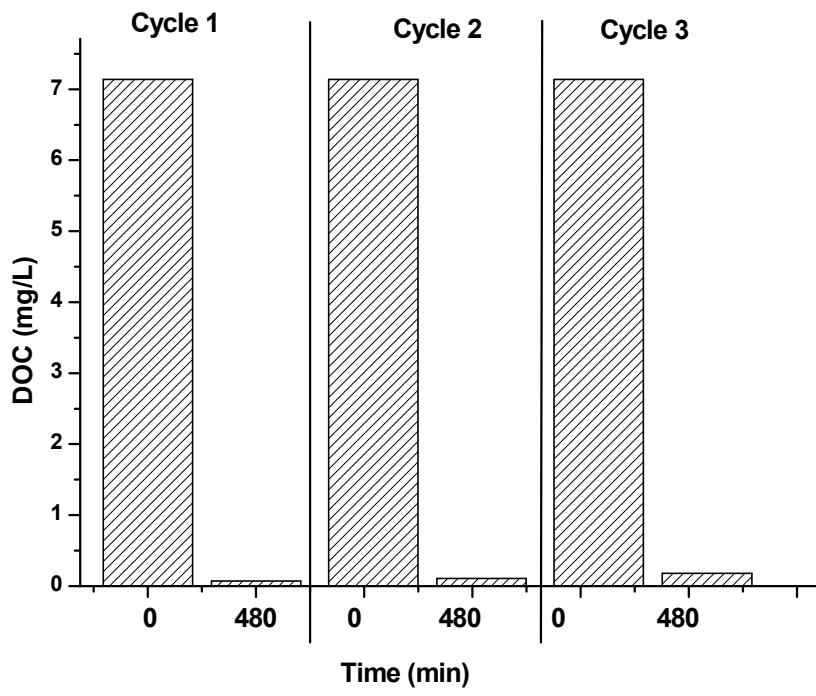
710

711 **Figure 13**
712



713
714

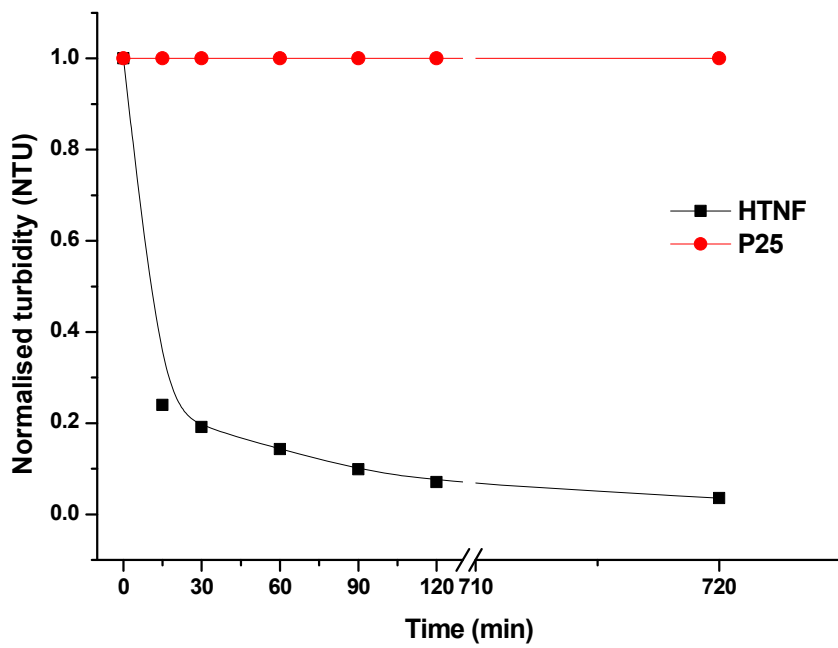
715 **Figure 14**



716

717

718 **Figure 15**



719
720
721

722 **List of Tables**

723

724 **Table 1.** Langmuir isotherm constants for MB adsorption onto HTNF under different
725 operating conditions.

726 **Table 2.** R_L values for different operational conditions.

727 **Table 3.** Regression equation and R^2 for MB discolouration against DOC removal.

728 **Table 4.** Apparent pseudo-first order kinetics for the photocatalytic degradation of MB over
729 HTNF under different operating conditions.

730

731

732

733

734

735

736

737

738

739

740

741

742

743

744

745

746

747

748

749

750

751

752

753

754

755

756 **Table 1**

757

Parameters	Operational conditions			
	HTNF Loading	MB concentration	pH	Temperature
$q_m(\text{mg/g})$	12	16.7	1.1	8.84
$k (\text{L/mg})$	5.5	30	0.08	0.17
R^2	0.91	0.99	0.89	0.99

758

759

760 **Table 2**

761

Operational conditions	HTNF loading (g/L)	MB concentration (mg/L)			pH	Temp (°C)
		5	10	20		
<i>R_L</i>	0.018	0.00002	0.028	0.001	0.37	0.22

762

763

764 **Table 3**

765

Parameter	Solution pH			
	3	7	5	9
Linear Regression equation	$y^{\S} = 0.489x^* + 0.547$	$y^{\S} = 0.668x^* + 0.272$	$y^{\S} = 0.677x^* + 0.244$	$y^{\S} = 0.753x^* + 0.188$
R^2	0.906	0.966	0.942	0.958

766 $\S y$ represents normalised DOC767 $*x$ represents normalised absorbance

768

769 **Table 4**

770

Parameter	Operational conditions						
	pH				Light Intensity		
	3	5	7	9	28000	15000	5000
$k^1_a(\text{min}^{-1})^\S$	0.011	0.025	0.037	0.034	same as pH 9	0.018	0.0037
R^2	0.994	0.828	0.915	0.893	same as pH 9	0.986	0.9440
$k^2_a(\text{min}^{-1})^*$	0.003	0.004	0.004	0.004	same as pH 9	0.003	0.002
R^2	0.979	0.820	0.888	0.735	same as pH 9	0.708	0.906

771 § Constants were calculated from the MB concentration degradation curves.772 * Constants were calculated from the DOC degradation curves to include the degradation of
773 intermediate compounds.

774

775